Published in final edited form as:
Cell Rep. 2013 July 11; 4(1): 66–75. doi:10.1016/j.celrep.2013.06.012.

FGF14 regulates presynaptic Ca^{2+} channels and synaptic transmission

Haidun Yan[1,3], **Juan L. Pablo**[2,3], and **Geoffrey S. Pitt**[1,2,3]

[1]Division of Cardiology, Department of Medicine, Duke University Medical Center, Durham, North Carolina 27710

[2]Department of Neurobiology, Duke University Medical Center, Durham, North Carolina 27710

[3]Ion Channel Research Unit; Duke University Medical Center, Durham, North Carolina 27710

SUMMARY

Fibroblast growth factor homologous factors (FHFs) are not growth factors, but instead bind to voltage-gated Na^+ channels (Na_V) and regulate their function. Mutations in *FGF14*, a FHF that is the locus for spinocerebellar ataxia 27 (SCA27) are believed pathogenic because of a dominant-negative reduction of Na_V currents in cerebellar granule cells. Here, we demonstrate that FGF14 also regulates members of the presynaptic Ca_V2 Ca^{2+} channel family. Knockdown of FGF14 in granule cells reduced Ca^{2+} currents and diminished vesicular recycling, a marker for presynaptic Ca^{2+} influx. As a consequence, excitatory post-synaptic currents (EPSCs) at the granule cell to Purkinje cell synapse were markedly diminished. Expression of the SCA27-causing *FGF14* mutant in granule cells exerted a dominant negative reduction in Ca^{2+} currents, vesicular recycling, and the resultant EPSCs in Purkinje cells. Thus, FHFs are multimodal, regulating several discrete neuronal signaling events. SCA27 likely results at least in part from dysregulation of Ca^{2+} channel function.

Introduction

The four members of the family of **f**ibroblast growth factor **h**omologous **f**actors (FHFs), a subset of the fibroblast growth factors (FHFs), have received increasing attention for their unanticipated modulation of voltage-gated Na^+ (Na_V) channels and regulation of neuronal excitability. Although FHFs acquired their name because of their homology to FGFs (Smallwood et al., 1996), several defining features set FHFs (FGF11-FGF14) apart from other FGFs. Most notably, lacking a signal sequence, FHFs are not secreted (Smallwood et al., 1996) and do not appear capable of functioning as growth factors (Olsen et al., 2003). Physiologic roles for FHFs remained ill-defined until a confluence of experiments identified FHFs as modulators of Na_V channels and regulators of neuronal signaling, and genetic data pinpointed *FGF14* as the locus for spinocerebellar ataxia 27 (SCA27).

Focus on FHF regulation of neuronal excitability began when *Fgf14*$^{-/-}$ mice showed ataxia (Wang et al., 2002), providing a basis for exploring the implications of a linkage analysis that identified a F150S missense mutation in “b” splice variant of *FGF14* (FGF14b^{F150S};

Correspondence to Geoffrey S. Pitt, Ion Channel Research Unit, Box 103030 Med Ctr, Duke University, Durham, NC 27710., Phone: 919-668-7641., Fax: 919-613-5145, geoffrey.pitt@duke.edu.

termed FGF14^{F145S} in some studies that used numbering based on the alternatively spliced FGF14a variant) as the etiology for the autosomal dominant SCA27 in an extended Dutch family (van Swieten et al., 2003). The specific mechanism(s) by which the human *FGF14* mutant or knockout of *Fgf14* in mouse affected neuronal signaling and led to ataxia were subsequently explained by the discovery of FGF12 as a binding partner for the C-terminus of $Na_V1.9$ via a yeast two-hybrid strategy (Liu et al., 2001). Several studies then showed that FHFs, through their interaction with Na_V C-termini, can modulate Na^+ channel currents (Liu et al., 2003; Lou et al., 2005). Moreover, the SCA27 missense mutant FGF14b^{F150S}, when expressed in cultured hippocampal neurons, decreased Na_V channel currents and depressed neuronal excitability in a dominant negative manner (Laezza et al., 2007). Ataxia phenotypes have also been associated with a frame-shift mutation causing early termination of FGF14 or a chromosomal translocation that disrupted *FGF14* (Dalski et al., 2005; Misceo et al., 2009). Some experiments hint that FGF14 can regulate other neuronal processes, however, such as synaptic transmission in hippocampal neurons (Xiao et al., 2007). How FGF14 contributes to these other signaling pathways are not known, and whether mechanisms other than Na^+ channel dysfunction contribute to the ataxia phenotype has not been examined.

Here, we focused on the role of FGF14 at the cerebellar granule cell to Purkinje cell synapse. We discovered that FGF14 in granule cells is a potent regulator of P/Q-type $Ca_V2.1$ Ca^{2+} channels, the dominant presynaptic Ca^{2+} channels in granule cells, and synaptic transmission. Further, the SCA27-causing mutant FGF14 impaired Ca_V channels in cerebellar neurons and affected synaptic transmission at the granule cell to Purkinje cell synapse. Thus, FGF14 is a regulator of multiple ionic currents and the pathogenic effects of mutant FGF14 are likely mediated by dysregulation of both Ca^{2+} channels and Na^+ channels.

Results

FGF14 affects Ca_V2 channels in cerebellar neurons

Although FGF14 regulates Na_V channel currents in granule cells (Goldfarb et al., 2007), we suspected that additional mechanisms might contribute to the SCA27 phenotype based on our observation that most SCA-associated channelopathies or the related episodic ataxias result from perturbed Ca^{2+} channel function (Shakkottai and Paulson, 2009) and with the observation that loss-of-function mutations in $Ca_V2.1$ underlie the ataxia phenotype in *tottering* mice (Fletcher et al., 1996). We therefore first asked whether FGF14 affected voltage-gated Ca^{2+} channels in granule cells within mixed primary rat cerebellar cultures containing both Purkinje cells and granule cells, which could be readily distinguished by their characteristic morphology and membrane capacitance (granule cell, 8.8 ± 0.2 pF, n=105; Purkinje cell, 15.4 ± 0.6 pF, n=50). To assess the effects of FGF14 on voltage-gated Ca^{2+} channels in granule cells, we recorded Ca^{2+} currents after FGF14 knockdown by shRNA.

A ramp protocol with 10 mM Ba^{2+} as the charge carrier, as shown in Figure 1A, revealed that FGF14 knockdown significantly reduced Ca^{2+} channel currents (summary data normalized to cell capacitance are shown in Figure 1B for FGF14 shRNA, scrambled shRNA, and a GFP transfection control). Peak inward Ba^{2+} currents were also elicited with a step protocol in which currents were evoked by a 500 ms voltage step from −80 mV to −10 mV, revealing that FGF14 knockdown significantly reduced Ca^{2+} channel current density (Figure 1C–D). We next assessed whether FGF14 affected influx through Ca^{2+} channels in response to an action potential waveform, by isolating the Cd^{2+}-sensitive integrated current. We found that knockdown of endogenous FGF14 by shRNA significantly decreased the integrated current compared to transfection with GFP or scrambled shRNA (Figure 1E–F).

The efficacy of the FGF14 shRNA construct was validated in hippocampal neurons, which (because they also express the related FGF13) allowed us to test specificity. Figure S1A shows effective knockdown of the axon initial segment (AIS)-enriched FGF14 by shRNA, but not by a scrambled control. FGF13, however, was unaffected (Figure S1B). The FGF14 shRNA, but not the scrambled control, also reduced FGF14 protein expressed in HEK293T cells (Figure S1C). After confirming efficacy and specificity of the FGF14 shRNA, we transfected it (or a scrambled control shRNA or GFP) into granule cells and recorded Ca^{2+} currents.

Since 95% of the somatodendritic Ca^{2+} current in granule cells is carried by $Ca_V2.1$ P/Q-type channels (Jun et al., 1999), as well as a similar fraction of presynaptic Ca^{2+} influx at the granule cell to Purkinje cell synapse (Mintz et al., 1995), we tested whether FGF14 specifically affected $Ca_V2.1$ P/Q Ca^{2+} channel currents in a heterologous expression system. The $Ca_V2.1$ pore-forming α_{1A} subunit along with the accessory β_2b and $\alpha_2\delta$ subunits were expressed in HEK293T cells and currents were evoked by step depolarizations with 10 mM Ba^{2+} as charge carrier (Figure 2A). The current-voltage (I–V) relationship shows that co-expression of FGF14b increased current density over a broad range of voltages (Figure 2B), without affecting kinetics of activation or steady-state inactivation (Figure S2A–B, Table 1). The integrated inward current through $Ca_V2.1$ in response to an action potential waveform also increased with FGF14 co-expression (Figure 2C–D). Co-expression of FGF14b also increased current density of the other major presynaptic Ca^{2+} channel, the $Ca_V2.2$ N-type channel (Figure 2E). In contrast, FGF14b did not affect the $Ca_V1.2$ L-type or $Ca_V2.3$ R-type channels, which are predominantly somatodendritic in location (Figure 2F–G). Together, these results showed that endogenous FGF14 affected granule cell Ca^{2+} channels and that FGF14 was capable of regulating the presynaptic $Ca_V2.1$ and $Ca_V2.2$ Ca^{2+} channels.

Because FGF14 did not affect $Ca_V2.1$ kinetics of activation or steady-state inactivation, we suspected that a major mechanism by which FGF14 increased current density was by increasing the number of channels at the plasma membrane. In HEK293T cells expressing $Ca_V2.1$ channels, we therefore measured the gating charge, with and without FGF14 co-expression, as a means to assess the number of channels at the cell surface. We isolated the gating charge by depolarizing the cell from a holding potential of −80 mV to the reversal potential (determined individually for each cell, average +43.2 mV ± 0.9 mV, n=27) and eliminated any remaining ionic current by blocking channels with Cd^{2+} (300 μM). Figure 3A–B shows that co-expression of FGF14b increased gating charge by ~ 35% compared to the GFP-only control, suggesting that FGF14b does increase the number of channels at the plasma membrane. This increase in gating charge could be attributed solely to the transfected $Ca_V2.1$ channels, and not to FGF14b effects upon endogenous ionic currents in HEK293T cells because transfection of FGF14b in the absence of $Ca_V2.1$ did not increase gating charge compared to cells transfected with GFP only (2.2 ±0.2 fC/pF, n=12; and 2.0 ± 0.3 fC/pF, n=10, respectively; $p>0.05$).

Presynaptic FGF14 regulates baseline transmission at the granule cell to Purkinje-cell synapse

Having established that FGF14 affects $Ca_V2.1$ channels, the predominant presynaptic Ca^{2+} channels at the granule cell to Purkinje cell synapse and since FGF14 is abundant in granule cell axons (Wang et al., 2002),we explored whether FGF14 affected synaptic transmission at the granule cell to Purkinje cell synapse. We used paired recordings to identify a granule cell to Purkinje cell synapse in which only the presynaptic granule cell was transfected with FGF14 shRNA, a scrambled control shRNA or GFP (Figure 4A). We then evoked unitary excitatory post-synaptic currents (EPSCs) in the presence of 20 μM (−) bicuculline. Knockdown of FGF14 in granule cells reduced the EPSC amplitude in Purkinje cells by more than 80% compared to EPSCs recorded from pairs in which the granule cell was

transfected with GFP only or with the control scrambled shRNA (Figure 4B–C). Because FGF14 is also present in Purkinje cell somata (Shakkottai et al., 2009), we also checked whether FGF14 exerted postsynaptic effects in Purkinje cells by examining glutamate- and GABA-evoked responses after knocking down endogenous FGF14 by shRNA. The glutamate- and GABA- evoked currents were obtained by directly application of drugs to Purkinje cells. We found that neither glutamate-nor GABA-evoked inward currents were altered compared to currents from Purkinje cells transfiected with a scrambled control shRNA or GFP only (Figure S3A–B), suggesting FGsF14 had no effect on post synaptic responses.

FGF14 regulates vesicular turnover and short-term synaptic plasticity

We hypothesized that FGF14 knockdown in granule cells reduced EPSCs at the granule cell to Purkinje cell synapse because of a diminished presynaptic Ca^{2+} current through $Ca_V2.1$ channels, consistent with the reduced $Ca_V2.1$ Ca^{2+} current seen in Figure 2. We therefore tested whether FGF14 might affect presynaptic Ca^{2+} influx in granule cells. We assessed this indirectly by two different means. First, we measured synaptic vesicular turnover after a 90 sec depolarization with 90 mM KCl. We measured turnover of synaptic vesicles with FM 4–64. The styryl FM dyes become trapped in vesicles that underwent endocytosis following synaptic activity (Ryan et al., 1993), providing a measure of vesicular turnover that is closely correlated with the amount of presynaptic Ca^{2+} influx (Evans and Cousin, 2007; Yamashita, 2012). We transfected the mixed cultures with shRNA to knockdown FGF14 or a scrambled control shRNA and quantified FM 4–64 usptake in granule cells after a 90 sec depolarization by 90 mM KCl. The styryl dye was included only during the 90 sec depolarization, after which the neurons were immediately washed then fixed. In these sparsely transfected cultures, we then followed a GFP-positive granule cell axon until it synapsed with an untransfected Purkinje cell and then counted the number of puncta positive for FM 4–64 and GFP fluorescence (Figure 5A). In all cases, quantification was performed with experimenter blinded to the identity of the transfection. Knockdown of FGF14 reduced the number of recycled punctae by 54 % compared to scrambled control shRNA (Figure 5B–C). Second, we assessed short term plasticity. Pre-synaptic Ca^{2+} influx plays an essential role in neurotransmitter release in central nervous system synapses, and also contributes to short-term synaptic plasticity. A reduction in presynaptic Ca^{2+} influx is predicted to increase the paired pulse ratio (PPR) in response to two closely spaced stimuli (Zucker and Regehr, 2002). In the presence of 20 μM (−) bicuculline, we measured the PPR in response to two stimuli at 10 Hz (Figure 5D–E) and found that when the granule cell expressed GFP only or the scrambled control shRNA, the PPR was near unity (1.03± 0.04, n=16; and 1.05 ± 0.06, n=10, respectively). Knockdown of FGF14, however, significantly increased the PPR (1.45 ± 0.11, n=27), consistent with an effect on presynaptic Ca^{2+} entry. Together with the reduction in vesicular turnover after FGF14 knockdown, these data provided corroborating evidence that presynaptic Ca^{2+} influx was reduced by FGF14 knockdown.

The SCA27-causing FGF14 mutant affects synaptic transmission in a dominant negative manner

We next addressed the effects of the $FGF14b^{F150S}$ mutant associated with SCA27. We chose the “b” splice variant for study, since it is the most abundantly expressed in brain (Wang et al., 2000). First, we examined whether $FGF14b^{F150S}$ affected voltage-gated Ca^{2+} channel currents (with 10 mM Ba^{2+} as a charge carrier) by step or ramp depolarization in granule cells. As seen in Figure 6A–D, transfection of $FGF14b^{F150S}$ significantly reduced Ca^{2+} channel current density. This decrease in Ca^{2+} current was also observed in response to an action potential waveform (Figure 6E–F). In contrast, overexpression of $FGF14b^{WT}$ markedly increased Ca^{2+} currents in response to a step depolarization, ramp protocol, or an

action potential waveform. Since FGF14 increased Ca^{2+} currents above control, these data suggest that the effects of endogenous FGF14 are not saturated (Figure 6A–F).

We next examined whether the $FGF14b^{F150S}$ mutant affected presynaptic Ca^{2+} influx in granule cells by using FM 4–64 labeled vesicular recycling as an indicator. Compared to control, the SCA27 mutant reduced vesicular recycling (Figure 7A–C). In contrast, overexpression of $FGF14b^{WT}$ increased vesicular recycling (Figure 7A–C), consistent with the observed effects on total Ca^{2+} current. Finally, we used paired recordings to measure EPSCs in Purkinje cells after stimulation of a granule cell transfected with $FGF14b^{F150S}$, allowing us to measure directly the effect of $FGF14b^{F150S}$ on synaptic transmission. As seen in Figure 7D–E, expression of $FGF14b^{F150S}$ in a granule cell exerted a dominant negative effect and markedly reduced the EPSCs amplitude in Purkinje cell by 63 %. Overexpression of $FGF14b^{WT}$, in contrast, markedly increased the EPSCs by 317 %, which also suggests that the effects of endogenous FGF14 were not saturating.

Discussion

Understanding of the physiological roles of FIEFs has greatly evolved since their initial discovery (Smallwood et al., 1996). Recognition of FHFs as Na_V channel binding partners and modulators, demonstration that *Fgf14*$^{-/-}$ mice displayed ataxia, identification of *FGF14* as the locus for SCA27, and demonstration that FIEFs cannot activate FGF receptors redirected most attention to the influence of FIEFs intracellularly and specifically focused attention on their roles in neuronal excitability (Liu et al., 2001; Liu et al., 2003; Olsen et al., 2003; van Swieten et al., 2003; Wang et al., 2002). Further focus on modulation of Na_V channels followed the demonstration that the SCA27 mutant version of FGF14 acted as a dominant negative to suppress Na_V currents and excitability in hippocampal neurons (Laezza et al., 2007) and that granule cells from *Fgf14*$^{-/-}$;*Fgf12*$^{-/-}$ mice displayed a deficit in intrinsic excitability and altered Na_V channel inactivation properties (Goldfarb et al., 2007). The ataxia phenotype common to *Fgf14*$^{-/-}$ mice and patients with the dominant negative $FGF14b^{F150S}$ mutation has thus been suspected to result from Na_V channel dysfunction in granule cells or Purkinje cells (Goldfarb et al., 2007; Shakkottai et al., 2009).

Nevertheless, several observations suggest that FIEFs might possess capabilities beyond Na_V channel regulation. For example, CA1 synapses in *Fgf14*$^{-/-}$ mice have fewer total and docked vesicles (Xiao et al., 2007) and *Fgf13* knockdown in *Xenopus* oocytes influences neuronal development by affecting bone morphogenetic protein receptor activation of the MEK5-ERK5 pathway (Nishimoto and Nishida, 2007). Moreover, certain FIEFs localize to the nucleus (Munoz-Sanjuan et al., 2000), a subcellular location in which FIEFs are unlikely to influence Na_V channels, and FIEFs appear to have binding partners other than Na_V channels, such as kinase scaffolds (Schoorlemmer and Goldfarb, 2001). In this context, our demonstration that FGF14 regulates $Ca_V2.1$ channel currents and synaptic transmission at the granule cell to Purkinje cell synapse adds an additional dimension to FHF function. How FGF14 affects these processes is unclear, but we suspect that mechanism differs from how FIEFs affect Na_V channels, for which there is direct binding with the Na_V C terminus (Wang et al., 2012). In contrast, we were unable to detect direct interactions between FGF14 and Ca_V2 channels by either co-immunoprecipitation or recombinant protein binding studies targeting intracellular domains of Ca_V2 channels or their auxiliary subunits. Consistent with our observations, FGF14 was not annotated as a component of the Ca_V2-anchored proteome in a recent analysis (Muller et al., 2010). Thus, we hypothesize that the FGF14 acts indirectly, or possibly transiently, to increase the number of Ca_V2 channels at the plasma membrane.

Importantly, our data provide a novel mechanism by which FGF14 could affect synaptic transmission at a granule cell to Purkinje cell synapse, thereby offering new insight into the etiology of the disease phenotypes in humans with SCA27 and the ataxia phenotype in *Fgf14*$^{-/-}$ mice. As we showed, the mutant FGF14b^{F150S} acts as a dominant negative, reducing Ca^{2+} channel currents in granule cells similar to the effect of shRNA knockdown of endogenous FGF14. The dominant-negative effect of FGF14b^{F150S} on Ca^{2+} currents in granule cells and the consequent reduction in EPSCs in Purkinje cells are both consistent with the observation that the mutant also acts as a dominant-negative to reduce Na^{+} channel currents in hippocampal neurons (Laezza et al., 2007). Our data measuring gating charge point to a potential role for FGF14 in trafficking Ca^{2+} channels to, or regulating removal from, the plasma membrane. As such, FHFs may have a broader role in trafficking ion channels, since we recently demonstrated that endogenous FGF13 increases the number of cell surface $Na_V1.5$ Na^{+} channels in cardiomyocytes (Wang et al., 2011). On the other hand, our data also underline the concept that individual FHFs confer channel-specific regulatory effects. For example, although FGF14 regulated $Ca_V2.1$ and $Ca_V2.2$, the major presynaptic Ca^{2+} channels, FGF14 did not affect currents through $Ca_V1.2$ or $Ca_V2.3$, which are mainly restricted to the somatodendritic compartments. Such data argue against the possibility that FGF14 mediates its effects via interaction with a Ca^{2+} channel auxiliary protein, which would be common to all Ca^{2+} channels, but could suggest that FGF14 controls a regulator, such as a kinase, that has effects specific to individual types of Ca^{2+} channels.

The FGF14b^{F150S}-induced reduction in Ca^{2+} channel currents fits well with the observation that most SCA-associated channelopathies or the related episodic ataxias result from perturbed Ca^{2+} channel function (Shakkottai and Paulson, 2009) and with the observation that loss-of-function mutations in $Ca_V2.1$ underlie the ataxia phenotype in *tottering* mice (Fletcher et al., 1996). Thus, the previously identified actions of FGF14 on granule cell Na_V currents (Goldfarb et al., 2007), together with its effects upon granule cell Ca_V currents and the consequences for Purkinje cell EPSCs described herein, suggest that altered Purkinje cell output from the cerebellum in *FGF14* loss-of-function or dominant negative mutations derives from multiple mechanisms. Along with the previously demonstrated FGF14b^{F150S}-dependent reduction in Na_V currents and channel availability (Laezza et al., 2007), these data suggest that FGF14 is truly multimodal and the ataxia phenotype caused by mutant FGF14 results from several independent mechanisms.

Experimental Procedures

Molecular Biology

Mouse FGF14b or FGF14b^{F150S} were cloned into pIRES2-AcGFP1. The F150S mutation in FGF14b was generated with QickChange (Agilent). Constructs were sequenced in both directions. A cDNA for $Ca_V2.1$ (Kraus et al., 1998) was kindly provided by A. Lee (U. Iowa) by permission of J. Striessnig (U. Innsbruck). A cDNA for $Ca_V2.3$ (Bannister et al., 2004) was kindly provided by Brett Adams (Utah State). The cDNAs for $Ca_V1.2$,β_2b and $\alpha_2\delta$ were previously described (Wang et al., 2007). Hairpins targeted to FGF14 were designed with Invitrogen's RNAi Designer. The sequences were synthesized via Integrated DNA Technologies and subsequently cloned into pLVTHM (Addgene). Neurons were transfected with the different constructs followed by immunocytochemical staining to determine the efficacy and specificity of knockdown. The most effective shRNA has the sequence 5' CGCGTGGAGGCAAACCAGTCAACAAGTGCATTCAAGAGATGCACTTGTTGACTG GTTTGC CTCCTTTTTTAT - 3' and was used for the experiments described in this work. A scrambled shRNA that exhibits no significant homology to genes in rodent genomes was used as a control. This scrambled shRNA has been previously described (Wang et al., 2011).

Primary Cerebellar Culture and transfection

Primary dissociated cerebellar cultures were prepared using minor modifications of a previously described procedure for preparation of hippocampal cultures (Wang et al., 2007). Briefly, the cerebellum cortex was dissected on ice from P0-P1 male or female Wistar rat pups, digested with 0.25% trypsin for 10 min at 37°C with Dulbecco's Modified Eagle's Medium (DMEM, Sigma), and dissociated into single cells by gentle trituration. The cells were seeded onto coverslips coated with 50 μg/ml poly-D-lysine (Sigma) and 25 μg/ml laminin (Sigma) at a density of $2.5–3.0\times10^5$ cells/coverslip (12 × 12 mm coverslip) in DMEM supplemented with 10% heat-inactivated fetal bovine serum (FBS). The cells were maintained in a humidified incubator in 5% CO_2 at 37°C. After 15–16h, the medium was replaced with Basal Medium Eagle (BME, Sigma) supplemented with 2% B27 (Invitrogen), 1% or 5% FBS, 25 μM uridine, 70 μM 5-fluorodeoxyuridine, and 20 mM KCl. After 5–7 days *in vitro* (DIV) culture, the neurons were transiently transfected with 1 μg plasmid DNA per coverslip with calcium phosphate, as described previously (Wang et al., 2007). Experiments were carried out 7–12 days after transfection.

HEK 293T Cell Culture and Transfection

Human embryonic kidney (HEK) 293T cells were maintained in DMEM containing 10% FBS at 37°C in a 5% CO_2 incubator. The cells were plated in 60-mm tissue culture dishes, grown to 65–75% confluency and transfected with Lipofectamine 2000 (Invitrogen) in serum-reduced medium (Opti-MEM; Invitrogen) following the manufacturer's instructions. The total amount of cDNA used per dish was 8 μg, which included 3 μg of $Ca_V2.1$, $Ca_V2.2$, $Ca_V2.3$, or $Ca_V1.2$ subunits (α_{1A}, α_{1B},α_{1E}, orα_{1C}, respectively); 2.2 μg of β_2b; 1.8 μg of $\alpha_2\delta$; 2 μg of the empty pIRES2-acGFP1 vector or FGF14b in 5 ml transfection medium. After 24h transfection, the cells were re- plated on coverslips coated with 50 μg/ml poly-D-lysine (Sigma) at a low density for recording.

Electrophysiological Recordings

Whole cell voltage-clamp recordings were obtained from cultured cerebellar granule cells and Purkinje cells 7–12 days after transfection. The granule cells and Purkinje cells were identified based on their size and morphology. For paired recording experiments, whole cell recordings used an Axopatch 200A and 200B amplifier (Axon Instruments, Inc., Union City, CA), the signal was filtered at 2 kHz to 5 kHz bandwidth. The data acquisition was performed using a DigiData 1322A (Axon Instruments, Inc) digitizer and stored on a personal computer running pClamp software, version 10. For EPSCs recording, patch pipettes with 5–6 MΩ resistances were filled with internal solution containing (in mM): 120 K-gluconate, 10 KCl, 5 $MgCl_2$, 0.6 EGTA, 5 HEPES, 10 phosphocreatine, 50U/ml creatine-phosphokinase, 2 Mg-ATP, and 0.2 GTP, pH 7.3 with KOH (290–300 mOsm). The external solution contained (in mM): 135 NaCl, 2 $CaCl_2$, 1 $MgCl_2$, 5 KCl, 10 glucose, and 5 HEPES, pH 7.3 with NaOH (300–310 mOsm). To block $GABA_A$ receptor activity, (−) bicuculline 20 μM was added to external solution. A brief 5 mV hyperpolarizing step was performed at the end of each sweep to monitor series resistance, capacitance, and input (leak) resistance throughout the experiment. Cells were rejected from analysis if the series resistance changed by >15~20 %. The neuronal Ca^{2+} currents were recorded using an EPC 10 USB patch amplifier (HEKA Elektronik, Lambrecht/Pfalz, Germany). The signal was filtered at 2.9 Hz and digitized at 20 Hz. To record currents through voltage-gated Ca^{2+} channels, we used a bath solution containing (in mM): 124 NaCl, 20 TEA-Cl, 1 $MgCl_2$, 10 $BaCl_2$, 5 HEPES, and 10 glucose, pH 7.3 with NaOH (300–310 mOsm). The internal solution contained (in mM): 115 CsCl, 20 TEA-Cl, 1 $CaCl_2$, 2 $MgCl_2$, 10 HEPES, and 2 Mg-ATP, pH 7.3 with CsOH (290–300 mOsm). To block Na^+ currents, 1μM Tetrodotoxin (TTX) was supplemented in external solution.

Whole cell voltage-clamp recordings were obtained from HEK293T cells at room temperature 2–3 days after transfection using external and internal solutions as described above. The liquid junction potential and series resistance for these recordings were not corrected, and cells were discarded if series resistance was more than 10 MΩ.

Protocols and data analysis

Data analysis was performed using PatchMaster, FitMaster, and Clampfit 10.2 software. All averaged data presented the mean ± SEM. Statistical significance was determined using Student's *t*- or one-way ANOVA tests. In whole-cell voltage-clamp mode, the unitary EPSCs were obtained by stimulating a transfected presynaptic granule cell and recording from a neighboring untransfected postsynaptic Purkinje cell 7–12 days after transfection (Figure 4A). To elicit unitary EPSCs, the two cells were both held at −70 mV membrane potential, and a 20 ms depolarization pulse was delivered to the granule cell. The EPSC amplitude was determined by an average of 5–10 EPSCs from each cell. The neuronal Ca^{2+} current was obtained by 500 ms step depolarization from a holding potential of −80 mV to −10 mV or by ramp from a holding potential of −80 mV to +50 mV in 1 sec. The current amplitude was normalized to each cell's capacitance.

Recombinant HEK293T cells were voltage-clamped at a holding potential (V_h) of −80 mV, and $Ca_V2.1$, $Ca_V2.2$, $Ca_V2.3$, or $Ca_V1.2$ current I_{Ca} was elicited by depolarizing pulses of 300 ms from −80 mV to +60 mV (in 10-mV increments). Peak I_{Ca} amplitude during the test pulse was divided by the corresponding cell capacitance to obtain a measure of current density (pA/pF). Current density-to-voltage relationships were plotted ($I-V$ relationship). $Ca_V2.1$ currents were also evoked by an action potential waveform command. The action potential waveform (APW) was modified from a previously reported study (Borst et al., 1995). In brief, the APW began at −80 mV and peaked at +33 mV with a 2-ms half-amplitude duration. The maximal rising and falling slopes were +127 V/s and −52 V/s, respectively. Ca^{2+} channel currents were defined as the $CdCI_2$ (300 μM) sensitive fraction. Gating charge was obtained by depolarization for holding potential (−80 mV) to the reversal potential (40–50 mV, determined individually for each cell) for 20 ms.

FM dye staining was performed on cultured cerebellar neurons. On day 6 (DIV), the neurons were transfected with pIRES2-AcGFP1 (Control), scrambled control shRNA, FGF14 shRNA, $FGF14b^{WT}$, or $FGF14b^{F150S}$. FM4-64 (Molecular Probes) dye loading was performed 9 days after transfection (15 DIV). The neurons were first washed in HBS (in mM) 139 NaCl, 2.5 KCl, 10 HEPES, 10 glucose, 2 $CaCl_2$, and 1.3 $MgCl_2$, pH 7.3 (300 mOsm), then depolarized for 90 s at room temperature with 90 mM KCl solution (in mM: 48.5 NaCl, 90 KCl, 10 glucose, 10 HEPES, 2 $CaCl_2$, 1.3 $MgCl_2$, 0.05 APV, and 0.02 DNQX) containing 15 μM FM4-64. The neurons were immediately washed for 2 min with a calcium-free HBS solution containing 0.1 mM Advasep-7 (Sigma) and then rinsed 3 times with HBS solution to remove all nonspecific membrane bound FM4-64. Finally, the cells were fixed for 10 min with 4% paraformaldehyde/4% sucrose.

Imaging was performed with a Zeiss LSM 510 confocal microscope using an oil immersion 40X objective. GFP and FM4-64 dye were excited at 488 and 543 nm, respectively. All images were collected at 1024 ×1024 pixel resolution. Nerve terminals of transfected neurons were identified by tracing the GFP-positive axons. Synaptic punctae incorporation along a traced axonal process was identified at a region away from the cell body. For quantification, the experimenter was blinded to the identity of the transfected plasmid. A 45 μm ×45 μm square region of interest was selected and the numbers of puncta were calculated using NIH ImageJ software. Particles <0.3 μm in diameter were excluded from analyses.

Supplementary Material

Refer to Web version on PubMed Central for supplementary material.

Acknowledgments

We thank Chaojian Wang for help generating the FGF14b^{WT} or FGF14b^{F150S} expression constructs in pIRES2-AcGFP1. This work was supported in part by NHLBI R01 HL71165 (G.S.P.).

References

Bannister RA, Melliti K, Adams BA. Differential modulation of CaV2.3 Ca2+ channels by Galphaq/11-coupled muscarinic receptors. Mol Pharmacol. 2004; 65:381–388. [PubMed: 14742680]

Borst JG, Helmchen F, Sakmann B. Pre- and postsynaptic whole-cell recordings in the medial nucleus of the trapezoid body of the rat. J Physiology. 1995; 489(Pt 3):825–840.

Dalski A, Atici J, Kreuz FR, Hellenbroich Y, Schwinger E, Zuhlke C. Mutation analysis in the fibroblast growth factor 14 gene: frameshift mutation and polymorphisms in patients with inherited ataxias. Eur J Hum Genet. 2005; 13:118–120. [PubMed: 15470364]

Evans GJ, Cousin MA. Simultaneous monitoring of three key neuronal functions in primary neuronal cultures. J Neurosci Methods. 2007; 160:197–205. [PubMed: 17049620]

Fletcher CF, Lutz CM, O'Sullivan TN, Shaughnessy JD Jr. Hawkes R, Frankel WN, Copeland NG, Jenkins NA. Absence epilepsy in tottering mutant mice is associated with calcium channel defects. Cell. 1996; 87:607–617. [PubMed: 8929530]

Goldfarb M, Schoorlemmer J, Williams A, Diwakar S, Wang Q, Huang X, Giza J, Tchetchik D, Kelley K, Vega A, et al. Fibroblast growth factor homologous factors control neuronal excitability through modulation of voltage-gated sodium channels. Neuron. 2007; 55:449–463. [PubMed: 17678857]

Jun K, Piedras-Renteria ES, Smith SM, Wheeler DB, Lee SB, Lee TG, Chin H, Adams ME, Scheller RH, Tsien RW, et al. Ablation of P/Q-type Ca2+ channel currents, altered synaptic transmission, and progressive ataxia in mice lacking the alpha 1A-subunit. Proceedings of the National Academy of Sciences. 1999; 96:15245–15250.

Kraus RL, Sinnegger MJ, Glossmann H, Hering S, Striessnig J. Familial hemiplegic migraine mutations change alpha1A Ca2+ channel kinetics. J Biol Chem. 1998; 273:5586–5590. [PubMed: 9488686]

Laezza F, Gerber BR, Lou JY, Kozel MA, Hartman H, Craig AM, Ornitz DM, Nerbonne JM. The FGF14(F145S) mutation disrupts the interaction of FGF14 with voltage-gated Na+ channels and impairs neuronal excitability. J Neurosci. 2007; 27:12033–12044. [PubMed: 17978045]

Liu C, Dib-Hajj SD, Waxman SG. Fibroblast growth factor homologous factor 1B binds to the C terminus of the tetrodotoxin-resistant sodium channel rNav1.9a (NaN). J Biol Chem. 2001; 276:18925–18933. [PubMed: 11376006]

Liu CJ, Dib-Hajj SD, Renganathan M, Cummins TR, Waxman SG. Modulation of the cardiac sodium channel Nav1.5 by fibroblast growth factor homologous factor 1B. J Biol Chem. 2003; 278:1029–1036. [PubMed: 12401812]

Lou JY, Laezza F, Gerber BR, Xiao M, Yamada KA, Hartmann H, Craig AM, Nerbonne JM, Ornitz DM. Fibroblast growth factor 14 is an intracellular modulator of voltage-gated sodium channels. J Physiol. 2005; 569:179–193. [PubMed: 16166153]

Mintz IM, Sabatini BL, Regehr WG. Calcium Control of Transmitter Release at a Cerebellar Synapse. Neuron. 1995; 15:675–688. [PubMed: 7546746]

Misceo D, Fannemel M, Baroy T, Roberto R, Tvedt B, Jaeger T, Bryn V, Stromme P, Frengen E. SCA27 caused by a chromosome translocation: further delineation of the phenotype. Neurogenetics. 2009; 10:371–374. [PubMed: 19471976]

Muller CS, Haupt A, Bildl W, Schindler J, Knaus HG, Meissner M, Rammner B, Striessnig J, Flockerzi V, Fakler B, et al. Quantitative proteomics of the Cav2 channel nano-environments in the mammalian brain. Proc Natl Acad Sci U S A. 2010; 107:14950–14957. [PubMed: 20668236]

Munoz-Sanjuan I, Smallwood PM, Nathans J. Isoform diversity among fibroblast growth factor homologous factors is generated by alternative promoter usage and differential splicing. J Biol Chem. 2000; 275:2589–2597. [PubMed: 10644718]

Nishimoto S, Nishida E. Fibroblast growth factor 13 is essential for neural differentiation in Xenopus early embryonic development. J Biol Chem. 2007; 282:24255–24261. [PubMed: 17584734]

Olsen SK, Garbi M, Zampieri N, Eliseenkova AV, Ornitz DM, Goldfarb M, Mohammadi M. Fibroblast growth factor (FGF) homologous factors share structural but not functional homology with FGFs. J Biol Chem. 2003; 278:34226–34236. [PubMed: 12815063]

Ryan TA, Reuter H, Wendland B, Schweizer FE, Tsien RW, Smith SJ. The Kinetics of Synaptic Vesicle Recycling Measured at Single Presynaptic Boutons. Neuron. 1993; 11:713–724. [PubMed: 8398156]

Schoorlemmer J, Goldfarb M. Fibroblast growth factor homologous factors are intracellular signaling proteins. Curr Biol. 2001; 11:793–797. [PubMed: 11378392]

Shakkottai VG, Paulson HL. Physiologic alterations in ataxia: channeling changes into novel therapies. Arch Neurol. 2009; 66:1196–1201. [PubMed: 19822774]

Shakkottai VG, Xiao M, Xu L, Wong M, Nerbonne JM, Ornitz DM, Yamada KA. FGF14 regulates the intrinsic excitability of cerebellar Purkinje neurons. Neurobiol Dis. 2009; 33:81–88. [PubMed: 18930825]

Smallwood PM, Munoz-Sanjuan I, Tong P, Macke JP, Hendry SH, Gilbert DJ, Copeland NG, Jenkins NA, Nathans J. Fibroblast growth factor (FGF) homologous factors: new members of the FGF family implicated in nervous system development. Proc Natl Acad Sci U S A. 1996; 93:9850–9857. [PubMed: 8790420]

van Swieten JC, Brusse E, de Graaf BM, Krieger E, van de Graaf R, de Koning I, Maat-Kievit A, Leegwater P, Dooijes D, Oostra BA, et al. A mutation in the fibroblast growth factor 14 gene is associated with autosomal dominant cerebellar ataxia [corrected]. Am J Hum Genet. 2003; 72:191–199. [PubMed: 12489043]

Wang C, Chung BC, Yan H, Lee SY, Pitt GS. Crystal structure of the ternary complex of a NaV C-terminal domain, a fibroblast growth factor homologous factor, and calmodulin. Structure. 2012; 20:1167–1176. [PubMed: 22705208]

Wang C, Hennessey JA, Kirkton RD, Wang C, Graham V, Puranam RS, Rosenberg PB, Bursac N, Pitt GS. Fibroblast growth factor homologous factor 13 regulates Na+ channels and conduction velocity in murine hearts. Circ Res. 2011; 109:775–782. [PubMed: 21817159]

Wang HG, George MS, Kim J, Wang C, Pitt GS. Ca2+/calmodulin regulates trafficking of Ca(V)1.2 Ca2+ channels in cultured hippocampal neurons. J Neurosci. 2007; 27:9086–9093. [PubMed: 17715345]

Wang Q, Bardgett ME, Wong M, Wozniak DF, Lou J, McNeil BD, Chen C, Nardi A, Reid DC, Yamada K, et al. Ataxia and paroxysmal dyskinesia in mice lacking axonally transported FGF14. Neuron. 2002; 35:25–38. [PubMed: 12123606]

Wang Q, McEwen DG, Ornitz DM. Subcellular and developmental expression of alternatively spliced forms of fibroblast growth factor 14. Mech Dev. 2000; 90:283–287. [PubMed: 10640713]

Xiao M, Xu L, Laezza F, Yamada K, Feng S, Ornitz DM. Impaired hippocampal synaptic transmission and plasticity in mice lacking fibroblast growth factor 14. Mol Cell Neurosci. 2007; 34:366–377. [PubMed: 17208450]

Yamashita T. Ca2+-dependent regulation of synaptic vesicle endocytosis. Neuroscience research. 2012; 73:1–7. [PubMed: 22401840]

Zucker RS, Regehr WG. SHORT-TERM SYNAPTIC PLASTICITY. Annual Review of Physiology. 2002; 64:355–405.

Highlights

- FGF14 regulates presynaptic CaV2.1 at the granule cell to Purkinje cell synapse
- FGF14 regulates presynaptic Ca^{2+} influx at the granule cell to Purkinje cell synapse
- FGF14 regulates synaptic transmission at the granule cell to Purkinje cell synapse
- Mutant FGF14 affects all these processes adversely

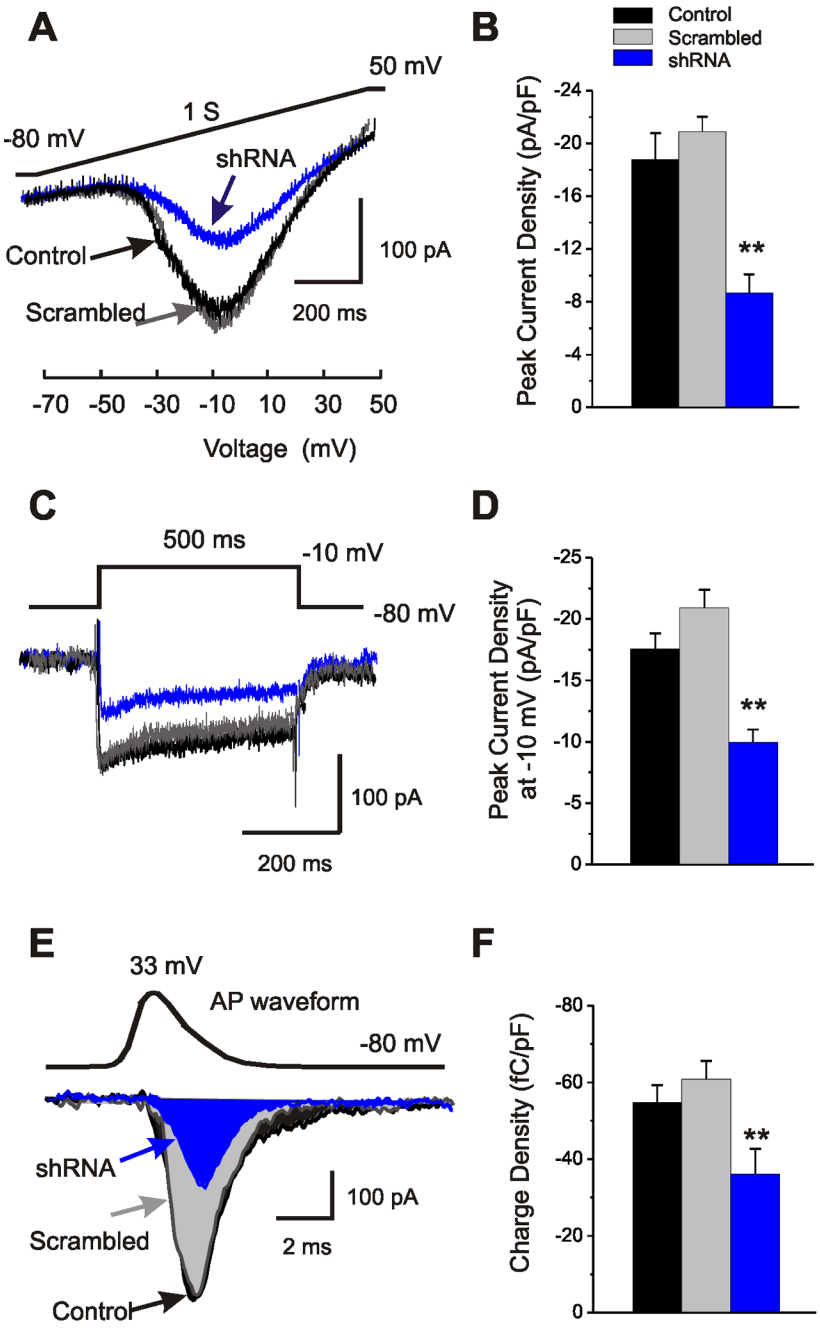

Figure 1. Endogenous FGF14 regulates Ca^{2+} channel currents in granule cells

A. Example Ca^{2+} channel current traces (using Ba^{2+} as the charge carrier) recorded from a cerebellar granule cell transfected with GFP-control (black), scrambled control shRNA (gray), or FGF14 shRNA (blue). The currents were evoked by a ramp protocol from a holding potential of −80 mV to 50 mV in 1 sec. **B**. Summary data from granule cells expressing GFP control (n=17), scrambled control shRNA (n=10), or FGF14 shRNA (n=12). **C**. Example Ca^{2+} channel current traces recorded from a cerebellar granule cell transfected with GFP-control (black), scrambled control shRNA (gray), or FGF14 shRNA (blue). The currents were evoked by a step protocol from a holding potential of −80 mV to

−10 mV in 500 ms. **D**. Summary data from granule cells expressing GFP control (n=22), scrambled control shRNA (n=11), or FGF14 shRNA (n=10). **E**. Representative Cd^{2+}-sensitive Ba^{2+} currents evoked by a single action potential waveform (APW, top) command recorded from granule cells transfected with GFP control (black), scrambled control shRNA (gray), or FGF14 shRNA (blue). The integrated current (Q) is colored with black, gray, or blue. **F**. Summary data of the integrated current (Q) normalized to each cell capacitance. Summary results were obtained from granule cells expressing GFP control (n=25), scrambled control shRNA (n=11), or FGF14 shRNA (n=10). **p<0.01 versus Control.

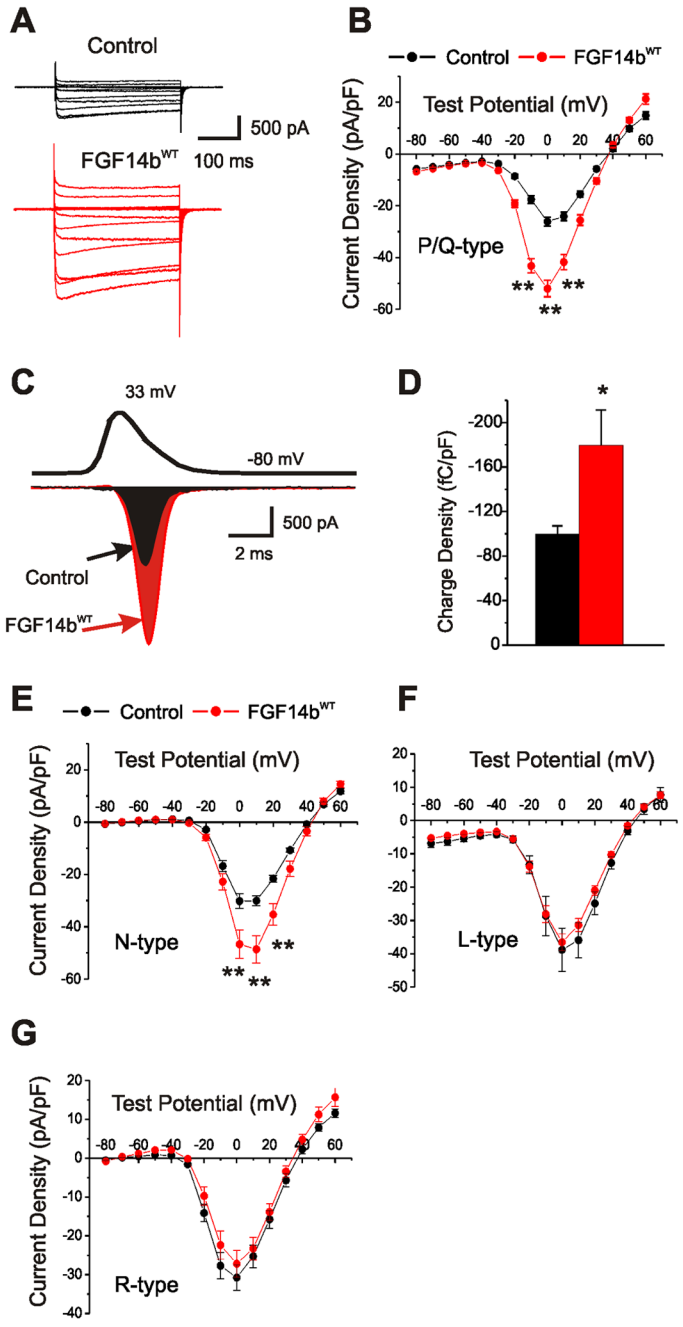

Figure 2. FGF14 modulates $Ca_V2.1$ and $Ca_V2.2$ channels

A. Example Ca^{2+} channel current traces (using Ba^{2+} as the charge carrier) recorded from HEK293T cells in which $Ca_V2.1$ channels were co-expressed with GFP control (black) or $FGF14^{WT}$ (red). The currents were elicited by depolarizing pulses of 300 ms from −80 mV to +60 mV (in 10-mV increments). **B**. Current-voltage relationships (normalized to cell capacitance) for cells in which $Ca_V2.1$ was co-transfected with GFP control (black) or $FGF14^{WT}$ (red). **C**. Representative Cd^{2+}-sensitive Ba^{2+} currents evoked by a single action potential waveform (APW, top) command from HEK293T cells in which $Ca_V2.1$ channels were co-transfected with GFP control (black) or $FGF14^{WT}$ (red). The integrated current (Q)

is colored with black or red. **D**. Summary data of the integrated current (Q) normalized to cell capacitance for each cell expressing GFP (n=9) or $FGF14^{WT}$ (n=9). **E-G**. Current-voltage relationships (normalized to cell capacitance) for cells in which $Ca_V2.2$ (E), $Ca_V1.2$ (F) or $Ca_V2.3$ (G) were co-transfected with GFP (black) or $FGF14^{WT}$ (red). The current amplitude values were divided by the capacitance of each cell to obtain current density (pA/pF). *$p<0.05$, **$p<0.01$ versus Control.

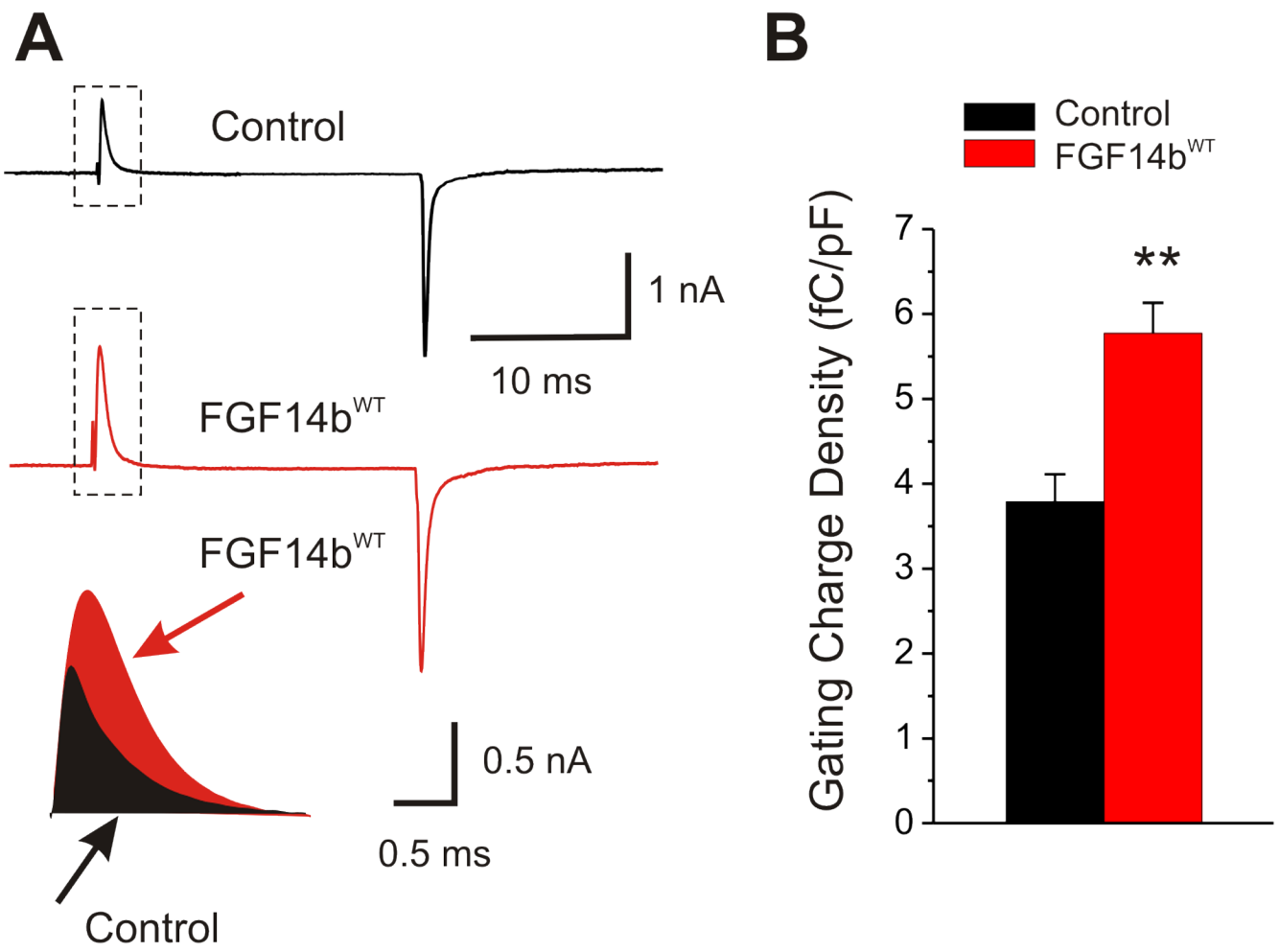

Figure 3. FGF14 increases Ca^{2+} gating charge in $Ca_V2.1$ channels

A. Example Ca^{2+} channel current traces (using Ba^{2+} as the charge carrier) recorded from HEK293T cells in which $Ca_V2.1$ channels were co-expressed with GFP control (black) or $FGF14^{WT}$ (red). The example traces were elicited by a 20 ms step from the holding potential (− 80 mV) to the reversal potential. Magnification of the integrated gating currents is shown below. **B**. Summary data of the integrated current (Q) normalized to each cell capacitance for cells expressing $Ca_V2.1$ or GFP control (n=14) or $FGF14^{WT}$ (n=13). **p<0.01 versus Control.

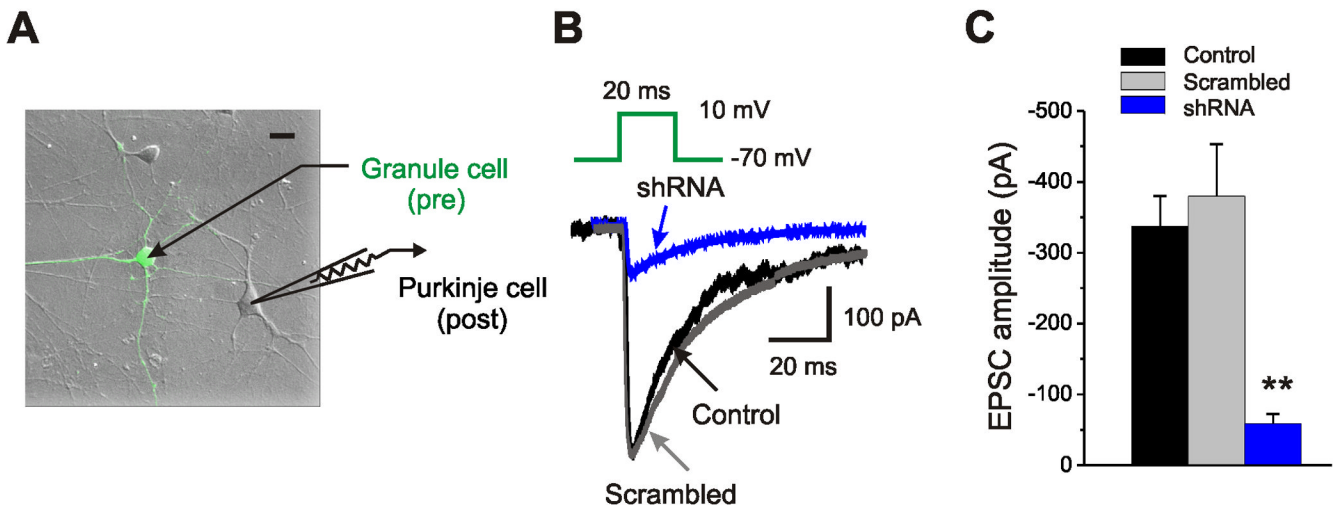

Figure 4. Endogenous FGF14 regulates synaptic transmission at the granule cell to Purkinje cell synapse

A. Evoked EPSCs in an untransfected Purkinje cell were elicited by a 20 ms depolarization of a transfected granule cell from a holding potential of −70 mV to −10 mV. **B**. Representative EPSC traces recorded from Purkinje cells in which the presynaptic granule cell was transfected with GFP control (black), scrambled control shRNA (gray), or FGF14 shRNA (blue). **C**. Averaged amplitude of unitary Purkinje cell EPSCs when the presynaptic granule cells expressed GFP control (n=14), scrambled control shRNA (n=25), or FGF14 shRNA (n=20). **p<0.01 versus Control.

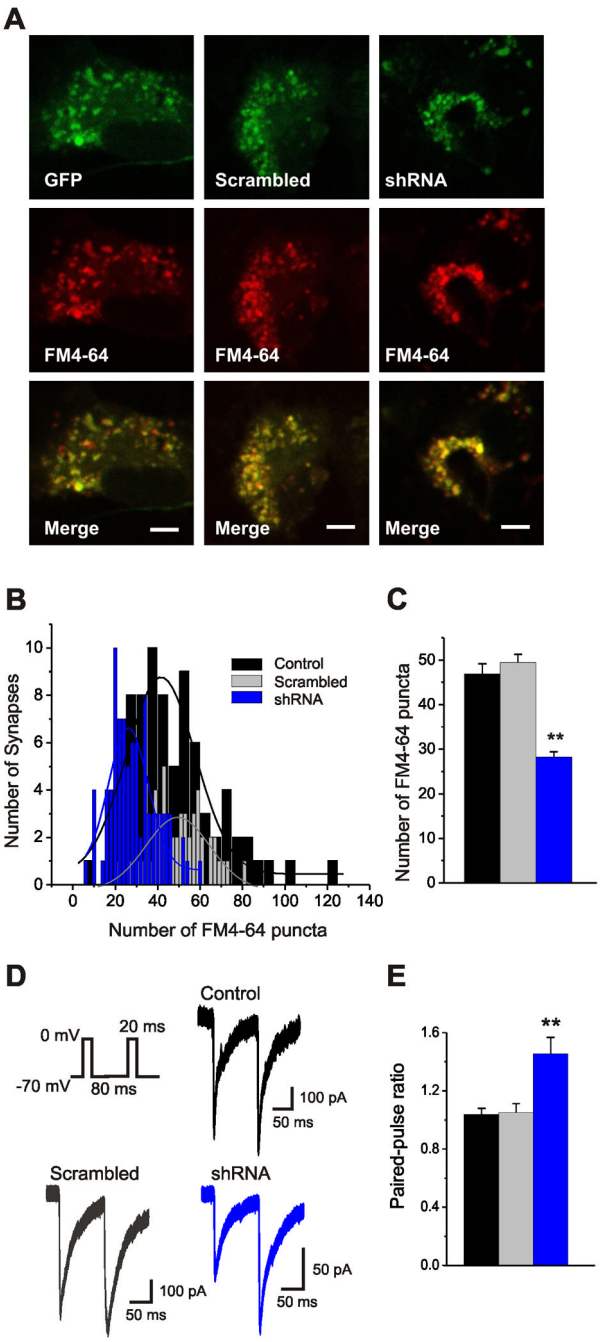

Figure 5. Endogenous FGF14 regulates vesicular recycling and short-term synaptic plasticity

A. Confocal images from cultured cerebellar neurons expressing GFP (left), scrambled control shRNA (middle), or FGF14 shRNA (right) that were loaded with FM4-64 by a 90 sec depolarization using 90 mM KCl. Scale bar, 5 μm. **B**. The distribution of FM4-64 puncta per synapse within a 45×45 μm^2 region of interest (ROI) in neurons transfected with control GFP (black, n=81), scrambled control shRNA (gray, n=49), or FGF14 shRNA (blue, n=87). The data for each group were fit to a Gaussian distribution. **C**. Average puncta per 45×45 μm^2 ROI for neurons over-expressing control GFP, scrambled control shRNA, or FGF14 shRNA. **D**. Representative EPSCs evoked by a paired-pulse protocol (indicated in inset; 80

ms interstimulus interval) when the presynaptic granule cells expressed GFP control (black), scrambled control shRNA (gray), or FGF14 shRNA (blue). **E**. Averaged paired-pulse ratio (amplitude of the second EPSC divided by the amplitude of the first EPSC). **p<0.01 versus Control.

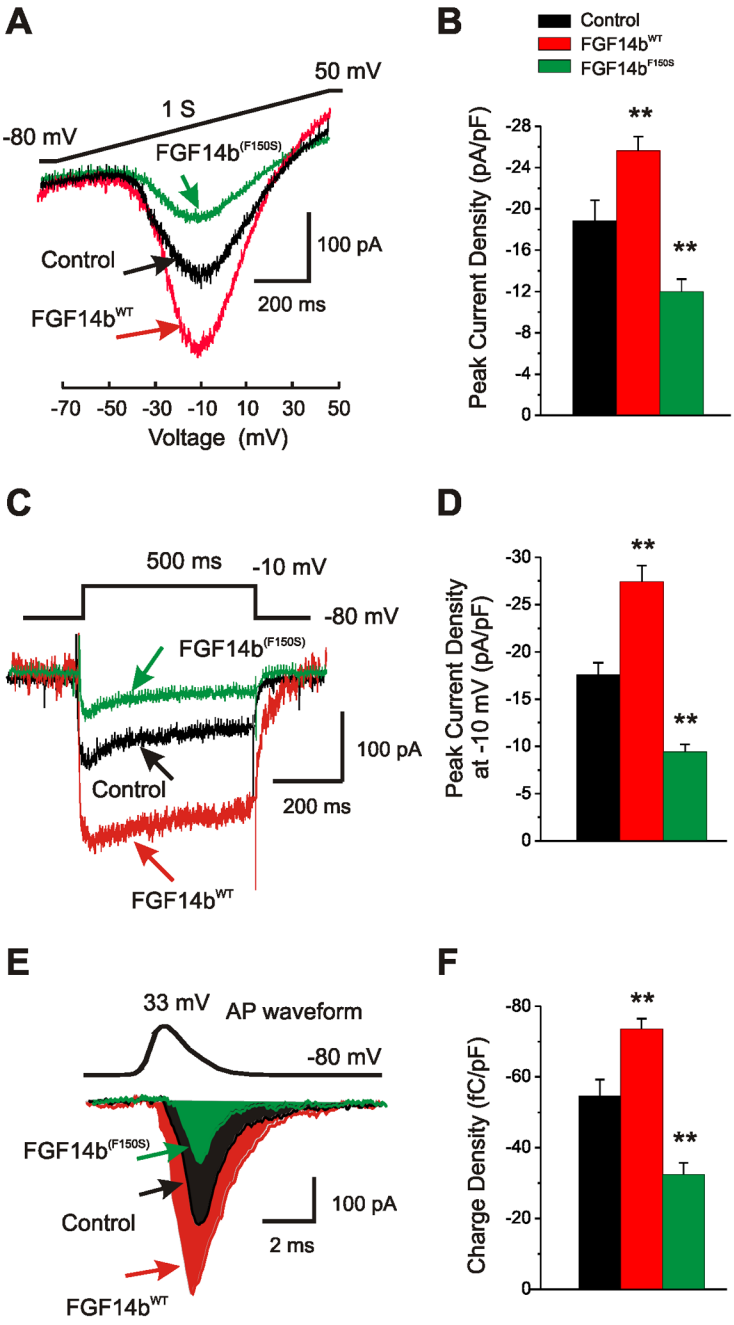

Figure 6. The SCA27 FGF14 mutant reduces granule Ca^{2+} currents

A. Example Ca^{2+} current traces (using Ba^{2+} as the charge carrier) recorded from a cerebellar granule cell transfected with GFP-control (black), $FGF14^{WT}$ (red), or $FGF14b^{F150S}$ (green). The currents were evoked by a ramp protocol from a holding potential of −80 mV to 50 mV in 1 sec. **B**. Summary data from granule cells expressing GFP control (n=17), $FGF14^{WT}$ (n=25), or $FGF14b^{F150S}$ (n=16). **C**. Example Ca^{2+} channel current traces recorded from a cerebellar granule cell transfected with GFP-control (black), $FGF14^{WT}$ (red), or $FGF14b^{F150S}$ (green). The currents were evoked by a step protocol from a holding potential of −80 mV to −10 mV in 500 ms. **D**. Summary data from granule cells expressing GFP

control (n=22), FGF14^{WT} (n=37), or FGF14b^{F150S} (n=13). **E**. Representative Cd^{2+}-sensitive Ba^{2+} currents evoked by a single action potential waveform (APW, top) command recorded from granule cells transfected with GFP control (black), scrambled control shRNA (gray), or FGF14 shRNA (blue). The integrated current (Q) is colored with black, red, or green. **F**. Summary data of the integrated current (Q) normalized to each cell capacitance. Summary results were obtained from granule cells expressing GFP control (n=25), FGF14^{WT} (n=28), or FGF14b^{F150S} (n=16). **p<0.01 versus Control.

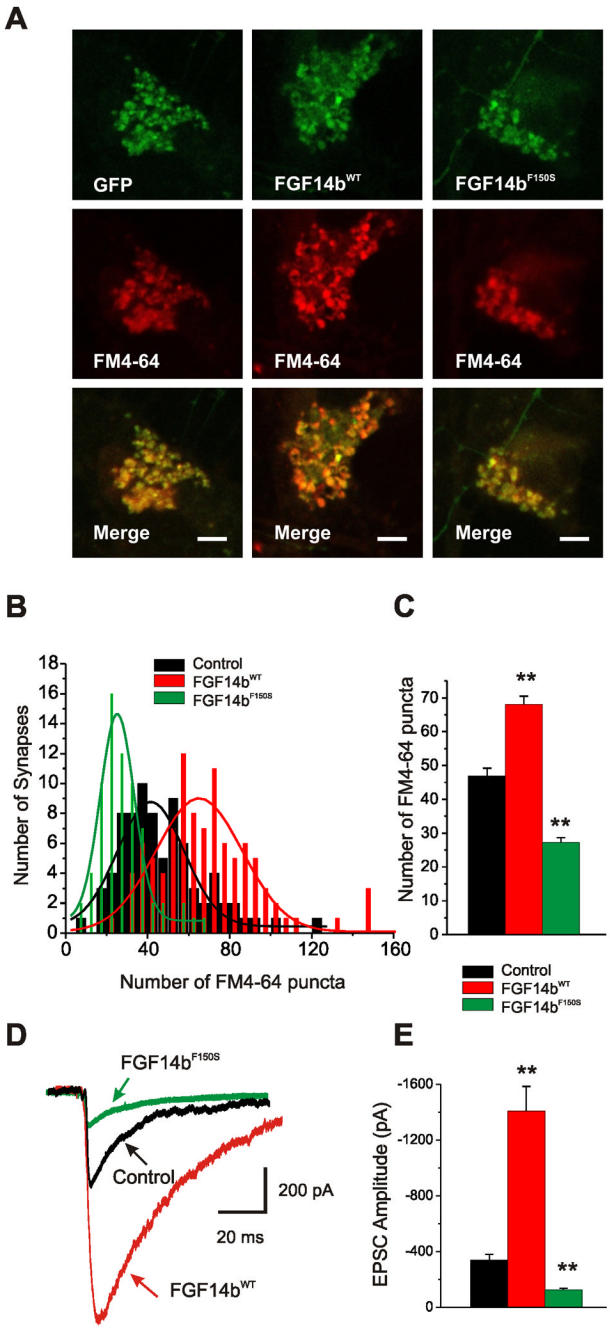

Figure 7. The SCA27 FGF14 mutant in granule cells reduces presynaptic Ca^{2+} influx and EPSCs at a granule cell to Purkinje cell synapse

A. Confocal images from cultured cerebellar neurons expressing GFP (left), $FGF14^{WT}$ (middle), or $FGF14b^{F150S}$ (right) that were loaded with FM4-64 by a 90 sec depolarization using 90 mM KCl. Scale bar, 5 μm. **B**. The distribution of FM4-64 puncta per synapse within a 45×45 μm^2 ROI in neurons transfected with GFP (black, n=81), $FGF14^{WT}$ (red, n=98), or $FGF14b^{F150S}$ (green, n=69). The data for each group were fit to a Gaussian distribution. **C**. Averaged puncta number per 45×45 μm^2 ROI for neurons over-expressing control GFP (black, n=81), $FGF14^{WT}$ (red, n=98), or $FGF14b^{F150S}$ (green, n=69). **D**. Representative EPSC traces recorded from Purkinje cells evoked by a 20 ms depolarization

of the granule cell from a holding potential of −70 mV to −10 mV in which the presynaptic granule cell was transfected with GFP (black), $FGF14^{WT}$ (red), or $FGF14b^{F150S}$ (green). **E**. Averaged amplitude of Purkinje cell EPSCs when the presynaptic granule cell expressed GFP control (n=14), $FGF14^{WT}$ (n=19), or $FGF14b^{F150S}$ (n=10). **p<0.01 versus Control.

Table 1

Summary electrophysiology data for $Ca_V2.1$ and $Ca_V2.2$ channel activation and inactivation in HEK293 cells

		$V_{1/2}$ (mV)	*K*	n
Activation				
$Ca_V2.1$	Control	−11.5 ± 0.9	5.9 ± 0.2	31
	$FGF14^{WT}$	−12.5 ± 0.5	5.4 ± 0.2	44
$Ca_V2.2$	Control	−4.8 ± 0.8	5.6 ± 0.2	24
	$FGF14^{WT}$	−5.2 ± 0.8	5.5 ± 0.2	25
Inactivation				
$Ca_V2.1$	Control	−19.3 ± 0.8	17.5 ± 1.4	23
	$FGF14^{WT}$	−18.2 ± 2.3	15.1 ± 0.6	20
$Ca_V2.2$	Control	−18.4 ± 1.5	14.8 ± 1.3	15
	$FGF14^{WT}$	−20.0 ±1.5	14.1 ± 0.6	14

Activation kinetics were obtained from fits with a Boltzmann equation of the form: $G=G_{max}/[1 + \exp(V - V_{1/2})/k]$, where G_{max} is the extrapolated maximum Ca^{2+} conductance, V is the test voltage, $V_{1/2}$ is the half-activation voltage, and *k* is the slope factor. Steady-state inactivation were obtained from fits with a Boltzmann relationship, $I/I_{max} = (1 + \exp((V - V_{1/2})/k))^{-1}$.